ADVANCED MATERIALS INTERFACES
Open Access
www.advmatinterfaces.de

Effect of Thermal Oxidation on the Structure, Surface Texturing, and Microstructure Evolution in Nanocrystalline Ga—O—N Films

*Debabrata Das, Francelia Sanchez, Paul Gaurav Nalam, Nolan Herbort, Felicia S. Manciu, V. Shutthanandan, and C.V. Ramana**

An extensive examination of the nanoscale, crystallographic growth dynamics of the system, which is impacted by the thermal energy given to the GaN, is carried out to derive a deeper understanding of the growth kinetics, morphology and microstructure evolution, chemical bonding, and optical properties of Ga—O—N films. Thermal annealing of GaN films is performed in the temperature range of 900–1200 °C. Crystal structure, phase formation, chemical composition, surface morphology, and microstructure evolution of Ga—O—N films are investigated as a function of temperature. Increasing temperature induces surface oxidation, which results in the formation of stable β-Ga_2O_3 phase in the GaN matrix, where the overall film composition evolves from nitride (GaN) to oxynitride (Ga—O—N). While GaN surfaces are smooth, planar, and featureless, oxidation induced granular-to-rod shaped morphology evolution is seen with increasing temperature to 1200 °C. The considerable texturing and stability of the nanocrystalline Ga—O—N on Si substrates can be attributed to the surface and interface driven modification because of thermal treatment. Corroborating with structure and chemical changes, Raman spectroscopic analyses also indicate that the chemical bonding evolution progresses from fully Ga—N bonds to Ga—O—N. While the GaN oxidation process starts with the formation of β-Ga_2O_3 at an annealing temperature of 1000 °C, higher annealing temperatures induce structural distortion with the potential formation of Ga—O—N bonds. The structure-phase-chemical composition correlation, which will be useful for nanocrystalline materials for selective optoelectronic applications, is established in Ga—O—N films made by thermal treatment of GaN.

1. Introduction

Conceptualizing and creating innovative materials that can exhibit better performance, scalability, and durability in challenging operational environments is of utmost importance in facilitating progress in many of the present and future technologies. The significance of this strategy is particularly crucial for developing technologies that operate at the intersection of several sectors and/or disciplines. Examples include ultraviolet photodetectors, photoelectrocatalysis, artificial photosynthesis, and photo-batteries, among many others.[1–5] In recent times, the scientific and engineering research community directed significant efforts into a range of wide/ultrawide bandgap (UWBG) material systems.[3,6–8] These materials include aluminum nitride (AlN), gallium nitride (GaN), zinc oxide (ZnO), hafnium oxide (HfO_2), lanthanum oxide (La_2O_3), germanium oxide (GeO_2), magnesium oxide (MgO), etc.[6–12] The primary objective of this exploration has been to push the boundaries of existing technological limits. Without question, contemporary research efforts related to UWBG

D. Das, F. Sanchez, P. G. Nalam, N. Herbort, C. Ramana
Center for Advanced Materials Research (CMR)
University of Texas at El Paso
500 W University Ave, El Paso, TX 79968, USA
E-mail: rvchintalapalle@utep.edu

The ORCID identification number(s) for the author(s) of this article can be found under https://doi.org/10.1002/admi.202400500

DOI: 10.1002/admi.202400500

F. Sanchez
Department of Metallurgical
Materials
and Biomedical Engineering
University of Texas at El Paso
500 W University Ave, El Paso, TX 79968, USA

P. G. Nalam, N. Herbort, V. Shutthanandan, C. Ramana
Department of Aerospace and Mechanical Engineering
University of Texas at El Paso
500 W University Ave, El Paso, TX 79968, USA

F. S. Manciu
Department of Physics
University of Texas at El Paso
500 W University Ave, El Paso, TX 79968, USA

V. Shutthanandan, C. Ramana
Pacific Northwest National Laboratory (PNNL)
Richland, WA 99352, USA

materials, and their alloys have showcased diverse methods for synthesizing and fabricating materials, as well as innovative designs. However, several inherent limitations exist in the methods/materials, which are suboptimal in terms of multifunctionality.

Unlike third-generation semiconductors, such as GaN and silicon carbide (SiC), gallium oxide (β-Ga_2O_3) offers various benefits, such as a broader bandgap, a stronger breakdown field, and the capacity to readily produce large-sized single crystals of superior quality.[13–18] Consequently, photodetectors based on β-Ga_2O_3 exhibit remarkable sensitivity and responsiveness within the deep-ultraviolet (DUV) spectrum, rendering them highly suitable for applications involving DUV sensing and imaging.[19–22] In addition, transistors based on β-Ga_2O_3 have demonstrated exceptional electron mobility, supporting them well-suited for electronic applications requiring high frequencies and high power.[15–18,23] Nevertheless, Ga_2O_3 unavoidably creates oxygen vacancies (V_O) throughout the development process, which provide substantial obstacles to intrinsic carrier management, p-type doping, and the establishment of stable Schottky connections.[13,18,24] For example, the existence of VO_O gives rise to persistent photoconductivity (PPC) phenomena, which give rise to unforeseen increases in photoconductivity but are accompanied by a sluggish reaction rate attributed to trapping effects.[25] In addition, the presence of V_O defects on the surface of Ga_2O_3 leads to the transportation of electrons by tunneling puncture effects, which in turn causes the transistors to experience a significant reverse leakage current.[14–18,25–26]

Reducing trapping states in Ga_2O_3 is crucial for enhancing the response speed of corresponding electronic and optoelectronic devices. Previous research has commonly identified the V_O defects situated near the bandgap as the primary cause of PPC effects, leading to the instability of oxide thin film transistors (TFTs) when exposed to light.[25] The use of nitrogen in oxides has been demonstrated as a successful method for decreasing the V_O density, resulting in significant enhancements in the electrical characteristics and operational dependability of oxide TFTs. Additionally, the use of anion engineering in oxynitrides presents a viable approach to enable modification of the electronic structure and electrical/optical properties.[24–30] The valence band maximum (VBM) is elevated due to the hybridization of N 2*p*, O 2*p*, and *p*-*d* repulsion induced by metal 3*d* orbitals.[24,29–30] This phenomenon effectively mitigates the PPC effect and reduces the bandgap of oxide contacts. While previous studies have shown that amorphous nitrogen-doped oxides and oxynitrides may produce high-performance TFTs and energy harvesting devices, there is a scarcity of reports on high-speed photodetectors achieved by including anion alloying in oxynitrides. Furthermore, the ability to tailor the chemical-composition, which ultimately results in chemical compounds with enhanced performance in various devices in addition to their applicability in energy storage and conversion technologies, generated strong interest in oxynitrides.

Gallium compounds, such as GaN, Ga_2O_3, and more recently, gallium oxynitrides ($GaON/Ga_3O_3N/Ga_xO_yN_z$), have been recognized for their ability to exhibit semiconducting and optoelectronic properties. Gallium-based compounds with different composition and materials in various morphologies have demonstrated significant use in a wide range of applications, such as high electron mobility transistors (HEMTs), UV-blue light emitting diodes and laser diodes, logic gates, field effect transistors (FETs), and sensing devices.[13–14,16,19–21] Although gallium oxynitride (Ga—O—N) compounds find application in numerous technologies, there is a scarcity of reports on their synthesis, structure-property correlation, and utilization. Studying the synthesis of Ga—O—N is highly exciting, and it will give a deeper understanding of the fundamental mechanisms, which in turn influence the properties and performance of the resulting materials. This is the impetus for the present work on Ga—O—N films resulting from GaN deposited on Si substrates. Furthermore, such fundamental studies are expected to create more opportunities to produce unique materials that can meet the requirements of a given technological application in the context of emerging electronics and optoelectronics. For instance, the use of a Ga-oxide and Ga-nitride system has been documented in the synthesis of a direct bandgap spinel structured gallium oxynitride (Ga_3O_3N) material, which has promising electrical characteristics.[31] In a similar vein, the creation of GaN thin films using a chemical technique involves the utilization of a metastable state for the cubic gallium oxynitride crystal phase material with a composition of $Ga_{2.8}O_{3.5}N_{0.5}$.[32]

The existing body of literature has demonstrated that Ga—O—N may be synthesized by the processes of oxidation, nitridation, and ammonolysis, utilizing both GaN and Ga_2O_3.[24,29,31–32] Several factors have not been fully understood in the formation of Ga—O—N through ammonolysis despite the observation of the complete growth of a Ga_2O_3 layer over a GaN crystal. The production of Ga—O—N poses a significant challenge because of several documented methods, including oxidation or nitridation, hydrothermal synthesis, sol-gel spin coating, and atomic layer deposition. However, it is important to note that these synthetic procedures have some limitations.[31–33] The hydrothermal and nitridation processes exhibit unpredictable composition, which poses challenges in optimizing performance and achieving high crystallinity. Oxidation of GaN is a commonly utilized method to demonstrate Ga—O—N thin films and nanostructures. This technique utilizes a reactive environment to facilitate chemical reactions and facilitate the development of films. The distinctive attribute of oxidation enables the application of films with customized characteristics, rendering them highly attractive to produce sophisticated semiconductor devices that possess specific performance criteria. Achieving the necessary features, such as bandgap engineering, carrier mobility, and optical qualities, in Ga—O—N films requires careful control over their composition, thickness, and uniformity. Therefore, this study focuses on examining the development of Ga—O—N thin films through systematic oxidation of sputtered GaN on Si substrates. **Figure 1** depicts the schematic of the specific approach and reaction mechanism employed to achieve Ga—O—N films from GaN. A thorough analysis of the crystallographic growth dynamics of the system, which is influenced by the thermal energy applied to the GaN, is conducted in order to provide insights into the growth kinetics and performance of Ga—O—N. Most importantly, we probed the chemical composition changes along with changes in the electronic band structure so as to derive a structure-chemistry-property correlation, which will facilitate the optimization of processing conditions to produce materials with desired structure, properties and performance. We observe an increased level of thermal stability in the surface oxide with β-Ga_2O_3 phase. This

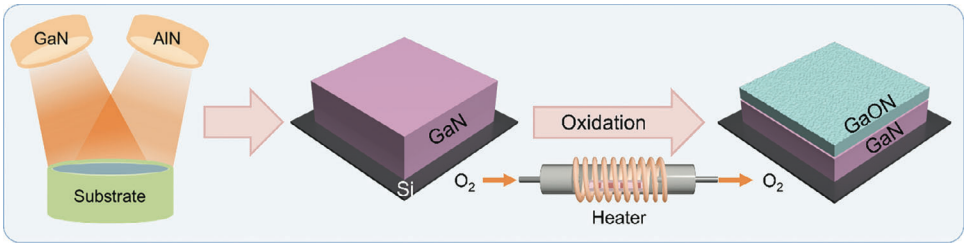

Figure 1. Schematic representation of Ga—O—N films' synthesis approach. Two-step process involved in the preparation of Ga—O—N thin films on Si substrates is schematically outlined. First, the deposition of 5 μm thick GaN films on Si with a thin AlN buffer layer is made. The second step is dry oxidation of GaN to synthesize Ga—O—N thin films.

may be attributed to the significant texturing and stabilization of the Ga—O—N on Si substrates, which is likely driven by the interface. The results obtained are presented and discussed in detail in this paper.

2. Results and Discussion

2.1. Crystal Structure, Phase, and Chemical Bonding

Figure 2 displays the XRD patterns of GaN. The data shown are for as grown, intrinsic GaN samples and GaN samples after undergoing thermal oxidation at a temperature ≥1000 °C. The as-deposited GaN/Si sample exhibits peaks corresponding to GaN (0002) along with a shoulder peak at the higher angle corresponding to the seed AlN (0002) layer.[34] This observation indicates the formation of the *c*-plane-oriented hexagonal phase of GaN films. The XRD peaks closely match the ones reported in the International Conference for Diffraction Data (ICDD) file 00-050-0792.[34] The additional phases are not present due to the growth of GaN on Si at a sufficiently high temperature of 725 °C, with AlN serving as a buffer layer. More specifically, under the optimum temperature (725 °C) of deposition hexagonal phase GaN formation occurs without any other GaN polymorphs, which may be induced or possible to grow at relatively lower or intermediate temperatures. The AlN buffer layer serves the objective of enhancing the surface shape/morphology and addressing the issue of significant lattice mismatch between GaN and Si. In addition, the samples exhibit Si (111) peak in the 2θ = 25–30° and peak corresponding 2nd harmonics at ≈58°.[34] Furthermore, when the GaN samples were subjected to thermal oxidation, evolution of distinct peaks associated with monoclinic β-Ga_2O_3 are seen. The peaks observed correspond to the diffraction from the ($\bar{2}$01), ($\bar{4}$02), ($\bar{6}$03), and (002) crystallographic planes, as compared to the ICDD file 01-074-1776.[35] The observed peaks exhibit a greater degree of significance, characterized by a rise in intensity when the oxidation temperature is increased. This suggests that a greater amount of oxide is produced as the oxidation temperature increases, and the thickness of the oxide grows as well.

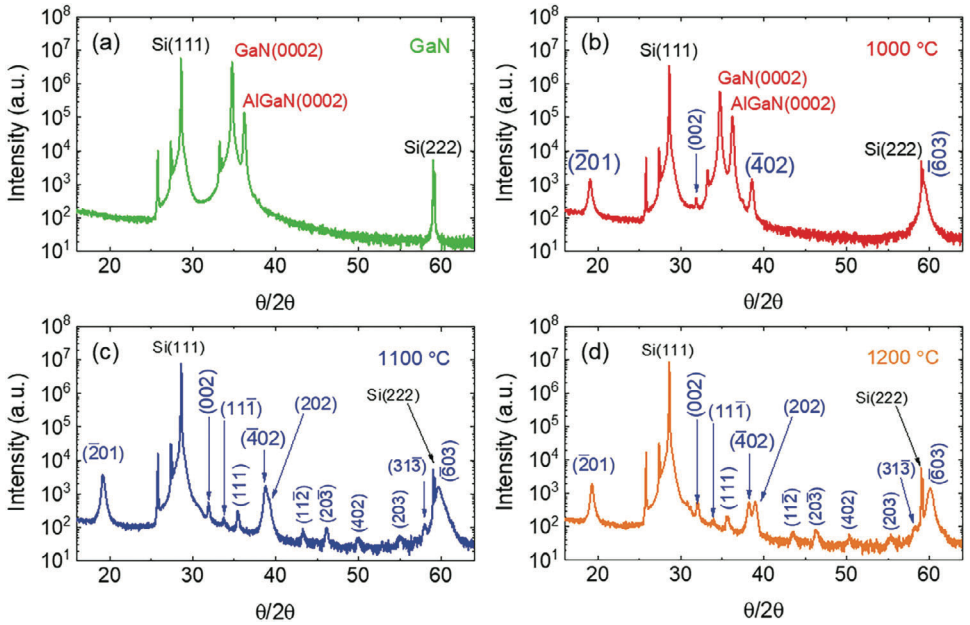

Figure 2. X-ray diffraction patterns of as-grown GaN (a) and oxidized Ga—O—N (b–d) thin films on Si substrate. Peaks correspond to Si, GaN, and Ga—O—N (β-$Ga_2(O_xN_{1-x})_3$) are shown in black, red, and blue color, respectively. Upon oxidation, the presence of monoclinic Ga—O—N is evidenced by the evolution of new peaks. The changes in terms of intensity increase of the new peaks indicate the increasing amount of Ga_2O_3 in the matrix with increasing temperature of oxidation. ICDD file numbers for GaN and Ga—O—N are 00-050-0792 and 01-074-1776.

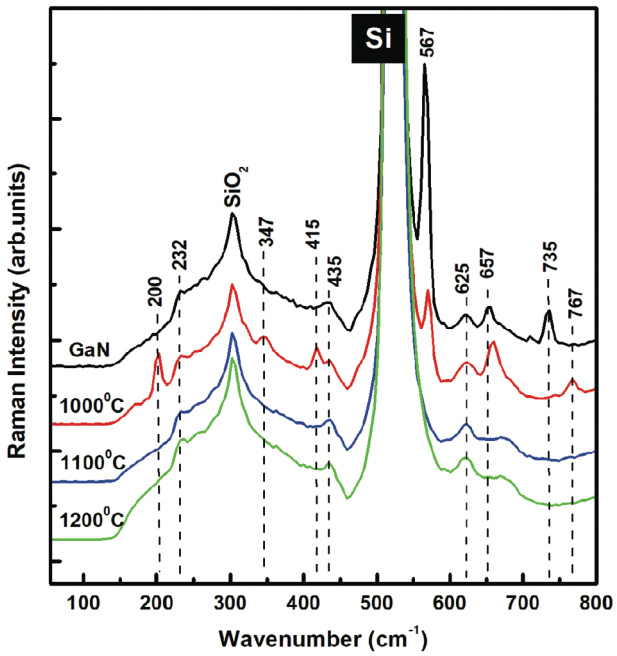

Figure 3. Raman spectra of Ga—O—N thin films. The data shown are as-grown GaN films on Si substrate and those annealed at various temperatures.

From 1100 °C onward, XRD results show additional peaks, such as (111), (402), (203), and (113), among others. This observation confirms that there is an extended probability of random orientation upon annealing at higher temperatures.

It is widely accepted that the monoclinic β-Ga_2O_3 has the highest thermodynamic stability among various polymorphs of Ga_2O_3.[13] Moreover, the occurrence of monoclinic β-Ga_2O_3 during thermal oxidation aligns with prior findings on the wet and dry oxidation of GaN in an air/oxygen environment. Nevertheless, several diffraction planes documented in previous research in the literature exhibit dissimilarities compared to our findings. For instance, Wolter et al. observed diffraction peaks in the $(\bar{2}02)$ and (311) planes when GaN underwent thermal oxidation in dry air.[36] Similarly, Kim et al. identified peaks due to diffraction from $(\bar{2}06)$ and $(\bar{3}06)$ planes when GaN underwent thermal oxidation in an oxygen-rich environment.[37] In contrast, Chen et al. and Zhou et al. observed peaks due to diffraction from the $(11\bar{3})$, $(30\bar{6})$, and $(\bar{1}13)$, $(\bar{3}06)$ planes, respectively, when GaN underwent thermal oxidation in a wet oxygen environment.[38,39]

We relied on Raman spectroscopy to further probe the chemical bonding changes in GaN under thermal oxidation. Raman spectroscopy has shown to be highly helpful in examining simple as well as complex materials, as it is a sensitive, productive, and nondestructive technique for examining a material's structure and chemical bonding over different length scales.[40,41] The Raman spectra of as-grown GaN film and GaN films annealed at various temperatures are presented in **Figure 3**. The spectra are translated vertically for easier comparison of potential changes induced by oxygen incorporation during the high-temperature annealing and oxidation process of GaN films. The strongest feature in the Raman spectrum of GaN is the peak at 567 cm^{-1} (E_2), followed by the 735 cm^{-1} (A_1) vibrational line that is associated with the longitudinal optical mode.[42] Besides a dominant signature of the Si substrate (as labeled), the peak at 303 cm^{-1} in this spectrum shows the presence of a thin SiO_2 layer. Other features, such as the weak shoulder at 232 cm^{-1} and the broad bands at 435 and 625 cm^{-1}, could also arise from the oxidation of the substrate. Another vibrational line at 657 cm^{-1} (E_2) is attributed to the AlN thin buffer layer used during the deposition of GaN.[42]

The annealing of the GaN film to 1000 °C induces significant modification in the film's structure. For example, a dramatic decrease in the GaN signature at 567 cm^{-1} and the disappearance of the 735 cm^{-1} line are observed. The new presence of a sharp peak at 200 cm^{-1} and three bands in the mid- and high-frequency region at 347, 415, and 767 cm^{-1} implies the formation of β-Ga_2O_3.[6,43–45] The intensity increase and slight blue shift by a few wavenumbers of the vibrational line at 657 cm^{-1} suggests a potential association of this feature with both AlN and gallium oxidation. Furthermore, its skewed shape toward the high-frequency side infers contribution from another weak and broad feature at ≈678 cm^{-1}, which can be better seen in the spectra of GaN film annealed at 1100 and 1200 °C. This latter remark indicates the potential formation of Ga—O—N bonds. While the GaN oxidation process starts with the formation of β-Ga_2O_3 at an annealing temperature of 1000 °C, higher annealing temperatures induce structure distortion and disorder, with potential formation of Ga—O—N bonds. This statement corroborates with the Raman bands seen in the 600–700 cm^{-1} region in the spectra of GaN annealed at 1100 and 1200 °C. The chemical bonding changes as a function of thermal oxidation temperature are further validated both qualitatively and quantitatively using XPS analyses.

2.2. Chemical Composition and Electronic Structure

Using XPS, we investigated the chemical and electronic structure changes as a function of temperature. The survey XPS spectra (**Figure 4a**) confirms the presence of Ga, N, and O by means of the respective peaks, which are exclusively due to these elements. Additionally, the C 1*s* peaks were also identified. These peaks are due to the absorption of carbon from the air exposure during the transfer of the samples to the XPS instrument. The adventitious C—C/C—H peak (284.8 eV) was used as a charge reference to calibrate the binding energy scale of the scans.[46]

The core level of spectra of Ga 3*d*, N 1*s*, and O 1*s* were analyzed in depth in order to probe the chemical changes on the GaN surface as a function of increasing temperature of oxidation. The asymmetric Ga 3*d* core level spectra shown in Figure 4b were conveniently deconvoluted into three $3d_{5/2}$ and $3d_{3/2}$ doublet components, which correspond to Ga—Ga, Ga—N, and Ga—O bonds.[26,47–53] The doublet peaks are constrained to have a 3:2 peak area ratio, equal full width half maxima (FWHM), and a fixed peak separation of 0.5 eV. In the as-grown GaN sample, the major component of the Ga 3*d* spectra is attributed to Ga—N bonds. Minor contributions of Ga—O and Ga—Ga are also observed. The metallic Ga—Ga bonds might be a result of N-vacancies on the surface, and the Ga—O can result from the oxidation of the metallic Ga.[26,49,54,55] An additional peak at lower binding energy (BE) is assigned to the emission of N 2*s* photoelectrons. Noticeably, with annealing, the gallium peaks shift to higher BE values as the spectra get dominated by Ga—O bonds.

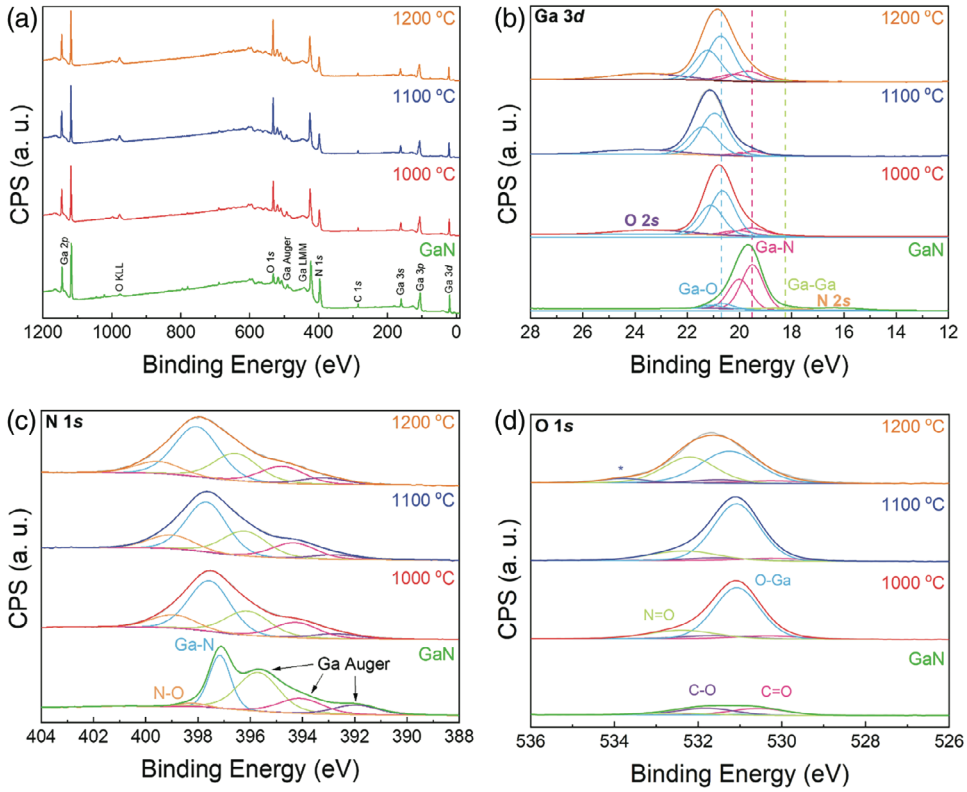

Figure 4. XPS data of thermally oxidized GaN samples. The data of as-deposited GaN are also shown for comparison. The data shown is: a) survey XPS spectra; b) the high-resolution Ga 3*d* core level spectra; c) the high-resolution N 1*s* core level spectra; and d) the high-resolution O 1*s* core level spectra.

Due to the higher oxygen incorporation, the N 2*s* region is suppressed, whereas the area of the O 2*s* peak increases with the annealing temperature. Moreover, oxygen annealing effectively removes any traces of metallic Ga—Ga bonds on the surface of the films.

The analysis of the N 1*s* spectra in Figure 4c is complex because of the overlapping position with the Ga Auger peaks (LMM region). The spectra were deconvoluted into Ga—N, N—O, and Ga Auger components.[47,49,51–53,55,56] The N 1*s* spectrum from as synthesized sample is dominated by Ga—N bonds. This observation is consistent with the fact that the initial set of samples are only GaN, which is expected to have the presence of only Ga—N bonds. However, the N—O bond in the non-treated sample is attributed to the oxygen adsorption onto the sample surface from air exposure. With annealing, the intensity of the N—O peak increases due to higher oxidation of the films. Further, the main Ga—N peak shifted to higher BE side as a result of the greater electronegativity of the oxygen atom (compared to the nitrogen atom) is attached.[49]

The high-resolution O 1*s* core level spectra in Figure 4d confirm the presence of oxides in the sample. The spectra are deconvoluted into C—O, C═O, Ga—O, and N—O components.[57] In the GaN sample, the O 1*s* region is dominated by carbon and oxygen bonds in the hydroxyl (C—O) and carbonyl (C═O groups that originate from adventitious carbon on the surface. After annealing, a strong peak centered at 531.1 eV is attributed to the Ga—O bonds of Ga_2O_3. The shoulder peak at 532.2 eV corresponds to N—O bonds. The origin of the additional peak at 533.8 eV from the sample annealed at 1200 °C is unknown, but it has been attributed to complex intermediate bonds between Ga—N—O.[53] Thus, the XPS studies reveal the most important aspect of GaN thermal oxidation, which always proceeds from surface of the GaN film and induces changes in Ga, O, and N concentration. The atomic concentration data of Ga, N, and O as a function of thermal oxidation temperature are shown in Figure S1 (Supporting Information), where it is evident that the surface oxygen concentration increases with increasing temperature. The relative changes in the concentration of these elements in their respective chemical bonds is presented in Figure S2 (Supporting Information). Again, it is evident that the surface Ga—N chemical bonds decrease while the Ga—O chemical bonds increase as thermal oxidation temperature increases. These results are in good agreement with the recent reports on GaN oxidation although the treatment procedures and range of temperatures are slightly varied.[28,58]

Detailed valence band spectrum (VBS) demonstrates the density of electronic states in the lowest BE region, and it provides the Fermi-level position relative to the VBM. We used the VB spectra of the as-deposited and thermally oxidized GaN samples in order to understand the electronic structure changes and to correlate the same with processing conditions. Specifically, we envision a drastic change in the VBS and VBM as the material progresses from GaN to Ga—O—N under thermal oxidation as seen in the aforementioned XRD and XPS analyses. As expected, upon thermal annealing, significant changes in the VBS can be noted as shown in **Figure 5**. The changes, which corroborate with

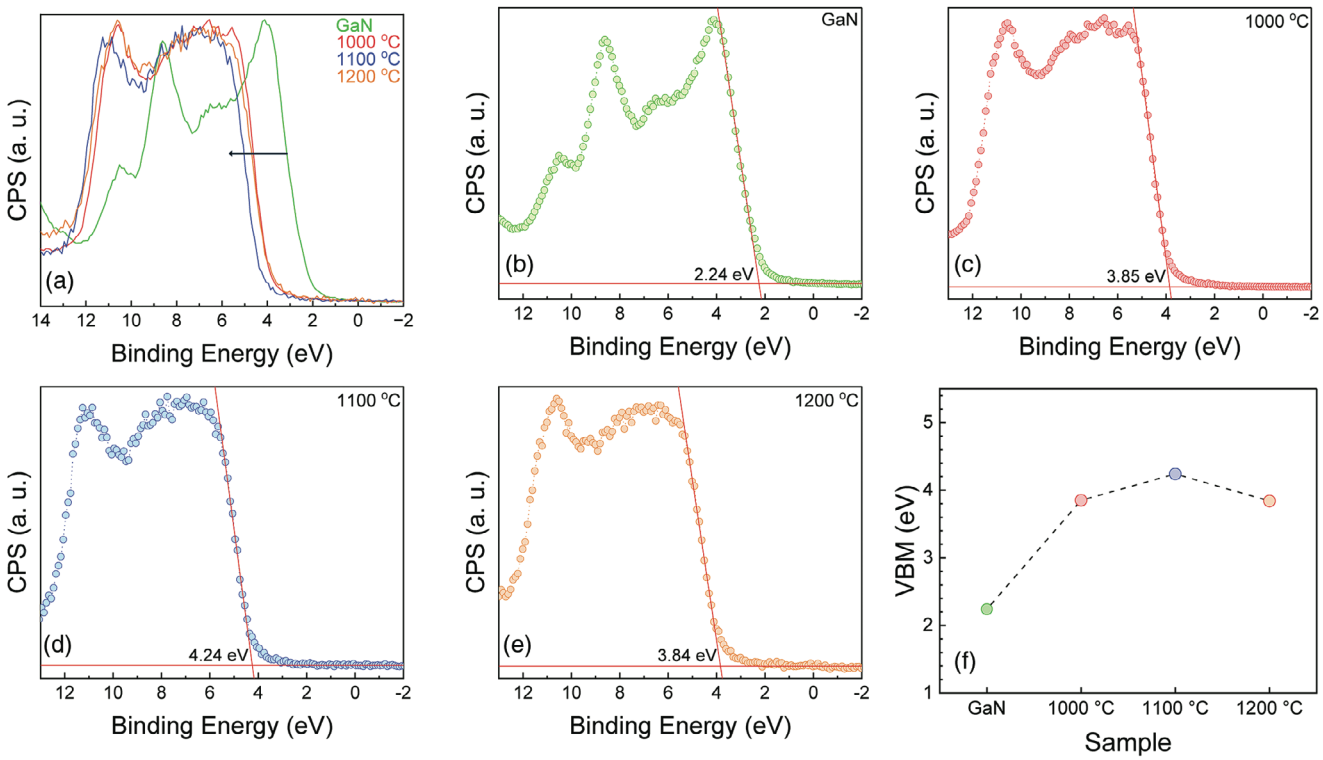

Figure 5. a–e) VBS of as-grown GaN and oxidized Ga—O—N thin films on Si substrate. f) Comparison of VBM values. It is evident from these plots that the samples exhibit a significant shift in VBM with increasing temperature. Also, the trend can be noted in (f) as the sample progress from GaN to Ga—O—N.

surface analysis by XPS, also suggest the formation of metal oxide at the surface of the GaN films. The position and shape of the VBS for the non-treated GaN (Figure 5b) are comparable to previous reports.[47] The VBS for GaN consists of Ga 4*p* to N 2*p* and Ga 4*s* to N 2*p* hybridized orbitals.[26,54,59] Nonetheless, thermally annealed GaN samples exhibit a characteristic VB spectrum of Ga_2O_3, which is dominated by Ga 4*p* and O 2*p* hybridized states (Figure 5c–e).[26,55] The VBM of the films was calculated from the linear extrapolation of the leading edge to the background line at zero counts in the VBS. The VBM of the films changes drastically with annealing due to the incorporation of oxygen. The changes in VBM can be understood as follows.

First, in intrinsic GaN, there is no effect of oxygen. The reported VBM values of GaN and Ga_2O_3 compounds are 2.27 and 4.05 eV, respectively.[21] The valance band maximum of non-annealed GaN film is 2.24 eV while annealed films have a VBM of ≈3.8–4.2 eV. The position and shape of the VBS for the as-grown GaN film are comparable to previous reports where the VBS consists of Ga 4*p* to N 2*p* and Ga 4*s* to N 2*p* hybridized orbitals.[54,56,59] However, the valence band spectra show notorious changes after annealing because of oxygen incorporation, and thus, the VBS is primarily composed of oxygen 2*p* orbitals. The drastic changes in VBM correlate with electronic structure changes with thermal oxidation. This is due to the fact that, the N 2*p* orbitals are typically at higher energy level than O 2*p* orbitals. The hybridization of higher energy N 2*p* orbitals with lower energy O 2*p* orbitals creates electronic states above the valence band and, hence, the consequence is the bandgap narrowing. Therefore, the strategy of nitridation is generally adopted in many of the oxide materials to introduce bandgap narrowing. However, the reverse effect is seen in GaN due to oxidation, where the O 2*p* orbitals hybridize with N 2*p* orbitals and increase bandgap. Perhaps, the effective hybridization of O 2*p* orbitals, which eventually span the entire valance band upon Ga_2O_3 formation, maybe the reason for the observed shift in VBM in Ga—O—N films under thermal annealing.

2.3. Morphology and Microstructure

After the detailed chemical and electronic structure analyses made using XPS and VBS, the microstructure and chemical composition evolution of the Ga—O—N samples was further probed by scanning electron microscopy (SEM) and energy dispersive X-ray spectrometry (EDS). It can be noted that the surface morphology of intrinsic GaN films prior to oxidation is fairly smooth without any indication of surface granular characteristics. However, with increasing temperature, the overall morphology (**Figure 6**) of the Ga—O—N samples demonstrates significant variation. The very first observation that can be made from SEM images is the emergence of the granular surface morphology upon thermal oxidation. Such surface morphology is clearly evident in Ga—O—N samples subjected to thermal oxidation at 1000 °C. Further increase in temperature causes the fully transformed rod-like morphology. This morphology of Ga—O—N films can be compared with bulk, polycrystalline Ga_2O_3 morphology (see, Figure S3, Supporting Information). Obviously, by comparing the SEM

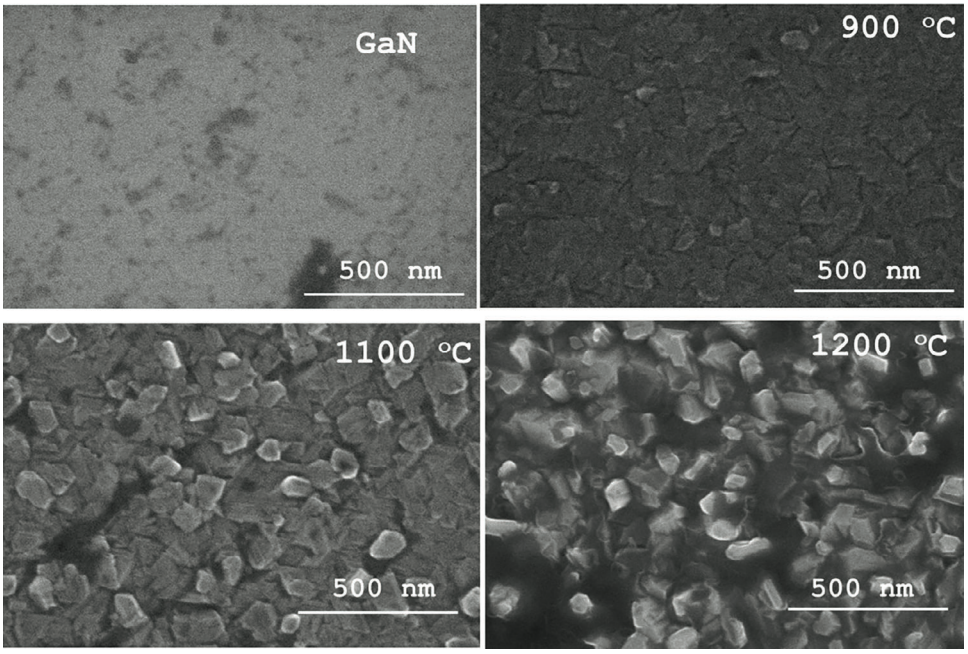

Figure 6. SEM images of as-grown GaN and oxidized Ga—O—N thin films on Si substrate. The emergence of granular morphology with thermal oxidation induced Ga—Oxide formation on the surfaces can be noted.

images of oxidized GaN samples with the bulk Ga_2O_3 polycrystalline sample, the morphology of the oxidized samples represents the characteristic of the emergence of the Ga-oxide phase on the GaN surface. Furthermore, quantitative analysis (using imageJ software) of the SEM data indicates that the granular size increases from ≈190 nm to ≈420 nm in diameter with increasing temperature. The EDS data (see Figure S4, Supporting Information) also confirms the chemical changes upon thermal oxidation. The chemical quality of the samples can be qualitatively discussed based on the EDS data since the chemical composition is reflected in the energy of the X-rays emitted. The X-ray energy is the characteristic of the atom from which the emission occurs.[60,61] The EDS data of GaN and Ga—O—N samples are presented in Figure S4 (Supporting Information). The elemental analysis exhibits the X-ray peaks due to Ga and N indicating the GaN prior to thermal oxidation. While the broad range EDS data are shown in Figure S4 (Supporting Information), the low-energy region, where the evolution of nitrogen and oxygen peaks are clearly seen is presented in **Figure 7**. It can be seen (Figure 7) that, upon oxidation, the nitrogen peak reduction occurs while the oxygen peak emerges. No presence of oxygen peak is seen in the EDS spectrum of the GaN sample prior to thermal oxidation. The oxygen peak evolves at 1000 °C while the presence of nitrogen is still seen. Finally, at 1200 °C, the nitrogen peak completely disappears while the oxygen peak intensifies. Thus, corroborating with XPS analyses, EDS data also confirms the formation of Ga-oxide on the surface upon thermal oxidation of GaN samples. Although the quantitative analysis of the EDS data may not be accurate for lighter elements, the details revealed by EDS for the chemical composition in atomic percentage are as follows. GaN films exhibit Ga:54.51; N:43.49; and O:2.10. While the nominal composition estimated is GaN, the minor concentration of oxygen is due to sample exposure to the environment. This observation is in good agreement with XPS results and analyses. At 900 °C, the EDS data indicate N:26.37 and O:12.57. At highest annealing temperature of 1200 °C, the EDS data show: N: 5.94 and O:34.65. Thus, the progressive changes seen in EDS are in good agreement with XPS results in terms of varying composition from GaN to Ga—O—N.

The emergence of granular type morphology seems to be a natural trend seen on the surfaces once the formation Ga-oxide proceeds onto the GaN upon thermal treatment. Liu et al. reported the granular structure formation on the GaN surfaces upon thermal oxidation.[28] The granular particle diameter increases with increasing temperature and finally transforms to the nanorod morphology. Similarly, most recently, Shi et al also reported the emergence of granular particles on the GaN surfaces upon thermal oxidation at 900 °C.[58] They observed that a further increase in oxidation temperature induces the increment in diameter, height, and density of granular particles. Increasing temperature to the higher end (1400 °C) induces significant changes in the surface morphology, where the rod-like structures continuously elongate, forming longer and more pronounced columns. These columns exhibit distinct edges and corners, indicating a monomorphic or polycrystalline structure, with a disordered growth direction. We also noted in our study on Sn-incorporated Ga—Sn—O samples that the increasing Sn concentration induces a significant shift in the samples' morphology. The surfaces are covered with deformed and shattered granules when Sn is incorporated. Thus, based on these observations and comparison with the literature, we propose that the surface oxidation of GaN proceeds with surface layers changing the chemical composition and morphology, where the predominantly observed morphology is the characteristic of the Ga-oxide formation. Furthermore, the XRD and XPS results, which are in good agreement with the SEM and EDS results, also support the

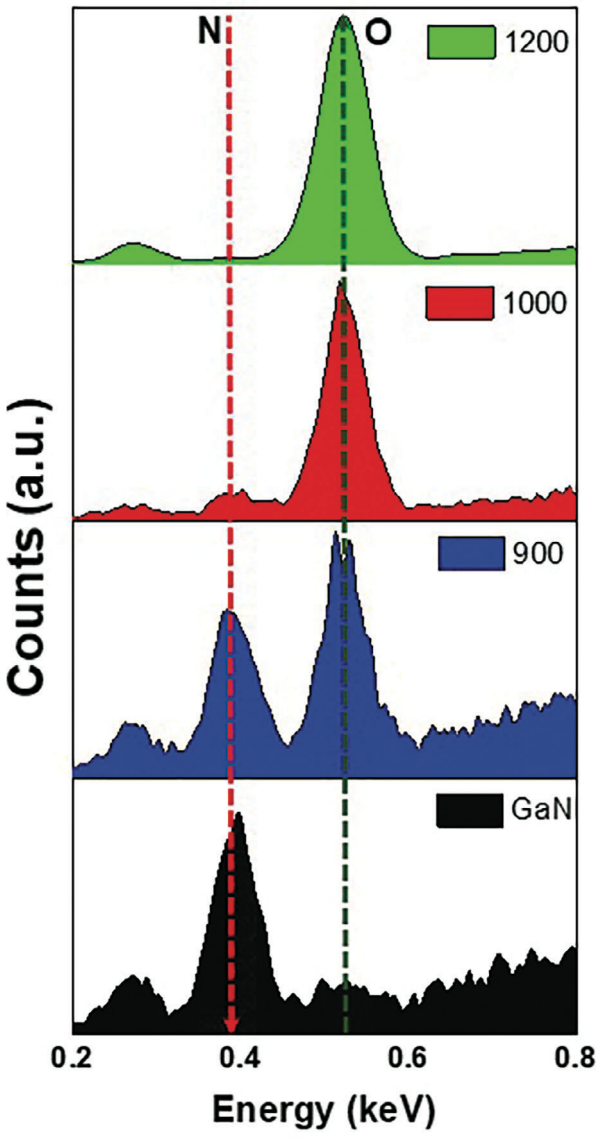

Figure 7. EDS data of GaN samples subjected the thermal oxidation. The low-energy region EDS spectra indicate the evolution of oxygen coupled with nitrogen peak reduction with thermal oxidation. Nitrogen peak almost disappears at the highest temperature (1200 °C) oxidation.

proposed mechanism, where gallium oxide formation occurs on the surface with the thermal oxidation process and when sufficient thermal energy is supplied by means of temperature.

3. Conclusion

We have conducted a comprehensive investigation on the oxidation of GaN films, formation of nanostructures, morphology of the surface/interface, electronic structure, and chemical composition. We have successfully shown that Ga—O—N thin films can be produced using a low-cost dry oxidation technique, with the ability to control their structural, chemical, and morphological characteristics. The studies reveal that, as the temperature rises, surface oxidation occurs, leading to the formation of a stable β-Ga_2O_3 phase in the GaN matrix. This is the transitional phase when the composition of the film changes from nitride (GaN) to oxynitride (Ga—O—N). Although GaN surfaces are smooth, planar, and featureless, oxidation-induced granular-to-rod-shaped morphological progression is seen when the temperature increases to 1200 °C. Heat treatment drives surface and interface transformation, which is responsible for the significant texturing and stability of the nanocrystalline Ga—O—N on Si substrates. In correlation with structure and morphology changes, the valence band structure also changes with thermal annealing due to the hybridization of the orbitals from nitrogen and oxygen. The valence band maximum shifts from 2.24 eV (GaN) to 4.24 eV (Ga—O—N) upon thermal oxidation accounting for the significant electronic structure modification upon Ga-oxide formation on the GaN surface. Raman spectroscopic studies also demonstrate that the chemical bonding development progresses from entirely Ga—N bonds to Ga—O—N bonds, which is consistent with structural and chemical modifications. While the GaN oxidation process begins with the creation of β-Ga_2O_3, higher annealing temperatures cause structural deformation induced by the formation of Ga—O—N bonds. The structure-phase-chemical composition correlation established in Ga—O—N films produced from thermal annealing of GaN will be helpful in tailoring the materials for optoelectronic applications.

4. Experimental Section

Synthesis of Nanostructured Ga—O—N Thin Films: A hybrid synthesis method (Figure 1) was introduced to produce nanostructured Ga—O—N films that can be controlled in their phase at the site. The method started with the deposition of GaN thin film onto Si(111) substrates, followed by further post-deposition processing in a controlled thermo-chemical environment. In post-deposition processing, the primary objective was to facilitate thermal oxidation and crystallization at varying temperatures.

Radio frequency magnetron sputtering was employed to deposit GaN films onto Si (111) substrates. The thin films were deposited using the DCSS12 radio frequency magnetron sputter system. Figure 1 displays a schematic diagram illustrating the deposition mechanism utilized for the production of GaN films. Prior to being introduced into the sputter chamber, the substrates underwent a meticulous cleaning process using acetone, methanol, and deionized water in a sequential manner, followed by dipping into buffered hydrofluoric acid and finally cleaning with deionized water. The deposition was conducted using 2″ pure GaN and AlN targets (Plasmaterial Inc.) with a purity of 99.999%. The base pressure of the sputter-deposition chamber was reduced to 1.5×10^{-7} mTorr prior to deposition by the exertion of a roughing pump and a turbo pump in series. The deposition process in the sputtering chamber involved the incorporation of Ar and N gas mixture (10:1) with a high purity level of 99.999%. The regulation of the gas flow rate was achieved by the utilization of MKS multi-gas controllers. Both the targets were ablated for 15 min each to remove any unwanted contamination. The substrate was heated up to 800 °C for 30 min to get rid of the oxide layer on top of the substrate. The actual deposition was done at 725 °C, which is well-established for the growth of GaN thin film. The deposition process was started with 50 nm thin AlN on Si to compensate for the overall strain further. After that, 5 µm thick GaN was deposited at the same substrate temperature. The plasma source power was regulated at 150 W. The deposition process was improved by maintaining a pressure of 1×10^{-2} mTorr and a substrate temperature of 725 °C. Prior to thermal oxidation, the GaN Film on a Si substrate with a thickness of 5 µm underwent RCA cleaning. The horizontal quartz tube furnace was utilized to conduct the thermal oxidation process. The temperature for oxidation is varied in the range of 900–1200 °C. To reach the oxidation temperature ≥1000 °C, a heating rate of 10 °C min^{-1} was employed in an ambient gas environment. The oxidation process was conducted in

an oxygen-ambient environment for a given duration of oxidation ranging from 120 min. Following the oxidation process, the samples were then cooled to ambient room temperature with a cooling rate of 10 °C min^{-1}.

Characterization—X-Ray Diffraction (XRD): The Ga—O—N thin films were subjected to X-ray diffraction studies using the Malvern Panalytical Empyrean Nano edition multifunctional X-ray diffractometer. The X-ray diffractometer was employed in the Bragg-Brentano reflection geometry. In order to achieve a distinct resolution of each peak observed in the diffraction pattern, Θ/2Θ scans were performed on the thin films at room temperature. The scans were done with a step size of 0.01° and an integration duration of 0.6 seconds per step. The observations were acquired using a copper potassium (Cu Kα) X-ray source with a wavelength of 0.154 nm. Prominent peaks originating from the silicon substrate were noticed. However, they have been omitted from the figures for the sake of convenience.

Characterization—Scanning Electron Microscopy (SEM): The surface morphology of the Ga—O—N samples was also probed using scanning electron microscopy (SEM). SEM measurements were conducted at room temperature using a Hitachi S-4800 (field emission) scanning electron microscope using an accelerating voltage of 15 kV.

Characterization—Energy Dispersive X-Ray Spectrometry (EDS): Energy dispersive X-ray spectrometry (EDS) was employed in order to comprehend the composition evolution in GaN samples as a function of oxidation. The backscattered electron mode was used for measurements, and scanning electron microscopy (SEM, Hitachi High-Tech America, Inc., USA) was used for the EDS measurements. Using x-ray color mapping in conjunction with elemental composition analysis, an approximate identification of the elements present and their distribution properties was made possible through the use of EDS.

Characterization—X-Ray Photoelectron Spectroscopy (XPS): The surface composition and chemical state of elements in the GaN and Ga—O—N films were measured using X-ray photoelectron spectroscopy (XPS). The XPS analyses were made on GaN/Ga—O—N films as a function of post-processing temperature. The measurements were conducted with a Thermo Fisher Scientific Nexsa spectrometer. The spectrometer was equipped with a focused Al Kα monochromatic x-ray source with a wavelength of 1486.6 eV. The spectrometer worked at a power of 72 W and had a high-resolution spherical mirror analyzer. The photoelectrons that were emitted were gathered at the entry slit of the analyzer, which was positioned perpendicular to the surface of the sample. The pressure in the analyzer chamber was consistently maintained at a value of 5×10^{-9} Torr. The spectral data for the survey was obtained by measuring the pass energy at 160 eV with a step size of 0.5 eV. Additionally, high-resolution spectra were obtained by measuring the pass energy at 50 eV with a step size of 0.1 eV. The Casa XPS program[62] was used to analyze the XPS data.

Characterization—Raman Spectroscopy: An alpha 300RAS WITec confocal Raman system (WITec GmbH, Ulm, Germany), using the 532 nm excitation of a Nd:YAG laser and a 20x objective (Nikon, Japan) with a numerical aperture NA = 0.4 was used for performing the Raman measurements. The microscope of the system was coupled via an optical fiber of 50 µm core diameter with a triple grating monochromator/spectrograph and a thermoelectrically cooled Marconi CCD camera. Accumulations of 20 spectra, with 500 ms acquisition time each, were co-added to improve the signal-to-noise ratio of every Raman spectrum recorded. A linear background subtraction and normalization to the Si peak intensity were applied. The latter was to account for potential variations in the laser power output, which was maintained at ≈5 mW.

Supporting Information

Supporting Information is available from the Wiley Online Library or from the author.

Acknowledgements

This material was based upon work supported by the Air Force Office of Scientific Research under award number FA9550-18-1-0387. However, any opinions, findings, conclusions, or recommendations expressed in this contribution are those of the author(s) and do not necessarily reflect the views of the United States Air Force. The authors also acknowledge, with pleasure, support from the National Science Foundation (NSF) with NSF-PREM grant #DMR-1827745. A portion of this research (Chemical Composition Analyses using X-ray Photoelectron Spectroscopy and Atom Probe Tomography) was performed on a project funded in part by a grant from the Washington State Department of Commerce's Clean Energy Fund and was also supported by the UTEP-PNNL Laboratory Directed Research and Development (LDRD) initiative at Pacific Northwest National Laboratory (PssNNL).

Conflict of Interest

The authors declare no conflict of interest.

Data Availability Statement

The data that support the findings of this study are available from the corresponding author upon reasonable request.

Keywords

chemical composition, GaN, Ga—O—N, microstructure, surface texturing

Received: June 6, 2024
Revised: October 2, 2024
Published online: January 16, 2025

[1] D.-H. Guan, X.-X. Wang, F. Li, L.-J. Zheng, M.-L. Li, H.-F. Wang, J.-J. Xu, *ACS Nano* **2022**, *16*, 12364.
[2] Y. H. Hong, Y.-M. Lee, W. Nam, S. Fukuzumi, *ACS Catal.* **2023**, *13*, 308.
[3] D. Das, F. Sanchez, D. J. Barton, S. Tan, V. Shutthanandan, A. Devaraj, C. V. Ramana, *Adv. Mater. Technol.* **2023**, *8*, 2300014.
[4] C. Wu, T. Zhao, H. He, H. Hu, Z. Liu, S. Wang, F. Zhang, Q. Wang, A. Liu, F. Wu, D. Guo, *Adv. Opt. Mater.* **2024**, *12*, 2302294.
[5] X. Sun, C. Wu, Y. Wang, D. Guo, *J. Vac. Sci. Technol. B* **2022**, *40*, 012204.
[6] N. Makeswaran, D. Das, V. Zade, P. Gaurav, V. Shutthanandan, S. Tan, C. V. Ramana, *ACS Appl. Nano Mater* **2021**, *4*, 3331.
[7] P. G. Nalam, D. Das, V. Shutthanandan, C. V. Ramana, *ACS Appl. Opt. Mater.* **2023**, *1*, 1761.
[8] P. G. Nalam, D. Das, S. Tan, C. V. Ramana, *ACS Appl. Electron. Mater.* **2022**, *4*, 3115.
[9] T.-J. Lu, B. Lienhard, K.-Y. Jeong, H. Moon, A. Iranmanesh, G. Grosso, D. Englund, *ACS Photonics* **2020**, *7*, 2650.
[10] M. J. Alam, P. Murkute, S. Sushama, H. Ghadi, S. Mondal, S. Paul, D. Das, S. K. Pandey, S. Chakrabarti, *J. Mater. Sci.: Mater. Electron.* **2020**, *31*, 18777.
[11] C. V. Ramana, K. K. Bharathi, A. Garcia, A. L. Campbell, *J. Phys. Chem. C* **2012**, *116*, 9955.
[12] V. V. Atuchin, A. V. Kalinkin, V. A. Kochubey, V. N. Kruchinin, R. S. Vemuri, C. V. Ramana, *Journal of Vacuum Science & Technology A* **2011**, *29*.
[13] S. J. Pearton, J. Yang, P. H. Cary, F. Ren, J. Kim, M. J. Tadjer, M. A. Mastro, *Appl. Phys. Rev.* **2018**, *5*, 011301.
[14] A. J. Green, J. Speck, G. Xing, P. Moens, F. Allerstam, K. Gumaelius, T. Neyer, A. Arias-Purdue, V. Mehrotra, A. Kuramata, K. Sasaki, S. Watanabe, K. Koshi, J. Blevins, O. Bierwagen, S.

Krishnamoorthy, K. Leedy, A. R. Arehart, A. T. Neal, S. Mou, S. A. Ringel, A. Kumar, A. Sharma, K. Ghosh, U. Singisetti, W. Li, K. Chabak, K. Liddy, A. Islam, S. Rajan, et al., *APL Mater.* **2022**, *10*, 029201.
[15] A. K. Rajapitamahuni, A. K. Manjeshwar, A. Kumar, A. Datta, P. Ranga, L. R. Thoutam, S. Krishnamoorthy, U. Singisetti, B. Jalan, *ACS Nano* **2022**, *16*, 8812.
[16] A. Mukherjee, V. Ottapilakkal, S. Sagar, B. C. Das, *ACS Appl. Nano Mater.* **2021**, *4*, 8050.
[17] B. Chatterjee, Y. Song, J. S. Lundh, Y. Zhang, Z. Xia, Z. Islam, J. Leach, C. McGray, P. Ranga, S. Krishnamoorthy, A. Haque, S. Rajan, S. Choi, *Appl. Phys. Lett.* **2020**, *117*, 153501.
[18] A. Bhattacharyya, C. Peterson, T. Itoh, S. Roy, J. Cooke, S. Rebollo, P. Ranga, B. Sensale-Rodriguez, S. Krishnamoorthy, *APL Mater.* **2023**, *11*, 021110.
[19] K. Arora, N. Goel, M. Kumar, M. Kumar, *ACS Photonics* **2018**, *5*, 2391.
[20] D. Guo, H. Liu, P. Li, Z. Wu, S. Wang, C. Cui, C. Li, W. Tang, *ACS Appl. Mater. Interfaces* **2017**, *9*, 1619.
[21] D. Guo, Y. Su, H. Shi, P. Li, N. Zhao, J. Ye, S. Wang, A. Liu, Z. Chen, C. Li, W. Tang, *ACS Nano* **2018**, *12*, 12827.
[22] F. Guo, B. Yang, Y. Yuan, Z. Xiao, Q. Dong, Y. Bi, J. Huang, *Nat. Nanotechnol.* **2012**, *7*, 798.
[23] Y. Qin, S. Long, Q. He, H. Dong, G. Jian, Y. Zhang, X. Hou, P. Tan, Z. Zhang, Y. Lu, C. Shan, J. Wang, W. Hu, H. Lv, Q. Liu, M. Liu, *Adv. Electron. Mater.* **2019**, *5*, 1900389.
[24] H. He, C. Wu, H. Hu, S. Wang, F. Zhang, D. Guo, F. Wu, *J. Phys. Chem. Lett.* **2023**, *14*, 6444.
[25] Z. Liu, L. Du, S. H. Zhang, L. Li, Z. Y. Xi, J. C. Tang, J. P. Fang, M. L. Zhang, L. L. Yang, S. Li, P. G. Li, Y. F. Guo, W. H. Tang, *IEEE Trans. Electron Devices* **2022**, *69*, 5595.
[26] S. K. Jain, P. Goel, U. Varshney, T. Garg, N. Aggarwal, S. Krishna, S. Singh, G. Gupta, *Appl. Surf. Sci. Adv.* **2021**, *5*, 100106.
[27] O. R. Nunez, A. J. Moreno Tarango, N. R. Murphy, C. V. Ramana, *J. Alloys Compd.* **2016**, *683*, 292.
[28] Y. Liu, S. Wei, C. Shan, M. Zhao, S.-Y. Lien, M.-k. Lee, *J. Mater. Res. Technol.* **2022**, *21*, 3113.
[29] Y. Zhang, X. Chen, Y. Xu, H. Gong, Y. Yang, F.-F. Ren, B. Liu, S. Gu, R. Zhang, J. Ye, *ACS Appl. Electron. Mater.* **2020**, *2*, 808.
[30] Y. Ma, T. Chen, X. Zhang, W. Tang, B. Feng, Y. Hu, L. Zhang, X. Zhou, X. Wei, K. Xu, D. Mudiyanselage, H. Fu, B. Zhang, *ACS Appl. Mater. Interfaces* **2022**, *14*, 35194.
[31] E. Soignard, D. Machon, P. F. McMillan, J. Dong, B. Xu, K. Leinenweber, *Chem. Mater.* **2005**, *17*, 5465.
[32] M. Puchinger, D. J. Kisailus, F. F. Lange, T. Wagner, *J. Cryst. Growth* **2002**, *245*, 219.
[33] P. Pedram, A. Zavabeti, N. Syed, A. Slassi, C. K. Nguyen, B. Fornacciari, A. Lamirand, J. Galipaud, A. Calzolari, R. Orobtchouk, A. Boes, T. Daeneke, S. Cueff, A. Mitchell, C. Monat, *Adv. Photonics Res.* **2024**, *5*, 2300252.
[34] M. Z. M. Yusoff, Z. Hassan, C. C. Woei, A. Ahmad, Y. Yusof, A. F. A. Rahim, 2012 IEEE Symposium on Business, Engineering and Industrial Applications **2012**.
[35] G. Gutierrez, E. M. Sundin, P. G. Nalam, V. Zade, R. Romero, A. N. Nair, S. Sreenivasan, D. Das, C. Li, C. V. Ramana, *J. Phys. Chem. C* **2021**, *125*, 20468.
[36] S. D. Wolter, S. E. Mohney, H. Venugopalan, D. L. Waltemyer, B. P. Luther, *MRS Online Proc. Libr.* **1997**, *468*, 495.
[37] H. Kim, S.-J. Park, H. Hwang, *J. Vac. Sci. Technol. B* **2001**, *19*, 579.
[38] P. Chen, R. Zhang, X. F. Xu, Z. Z. Chen, Y. G. Zhou, S. Y. Xie, Y. Shi, B. Shen, S. L. Gu, Z. C. Huang, J. Hu, Y. D. Zheng, *MRS Internet J. Nitride Semicond. Res.* **2000**, *5*, 866.
[39] Y. Zhou, C. Ahyi, T. Isaacs-Smith, M. Bozack, C.-C. Tin, J. Williams, M. Park, A.-j. Cheng, J.-H. Park, D.-J. Kim, D. Wang, E. A. Preble, A. Hanser, K. Evans, *Solid·State Electron.* **2008**, *52*, 756.
[40] V. S. Puli, D. K. Pradhan, S. Adireddy, R. Martínez, P. Silwal, J. F. Scott, C. V. Ramana, D. B. Chrisey, R. S. Katiyar, *J. Phys. D: Appl. Phys.* **2015**, *48*, 355502.
[41] C. V. Ramana, A. Mauger, C. M. Julien, *Prog. Cryst. Growth Charact. Mater.* **2021**, *67*, 100533.
[42] V. Y. Davydov, Y. E. Kitaev, I. N. Goncharuk, A. N. Smirnov, J. Graul, O. Semchinova, D. Uffmann, M. B. Smirnov, A. P. Mirgorodsky, R. A. Evarestov, *Phys. Rev. B* **1998**, *58*, 12899.
[43] D. Das, G. Gutierrez, C. V. Ramana, *ACS Omega* **2023**, *8*, 11709.
[44] S. Roy, C. V. Ramana, *J. Mater. Sci. Technol.* **2021**, *67*, 135.
[45] R. Rao, A. M. Rao, B. Xu, J. Dong, S. Sharma, M. K. Sunkara, *J. Appl. Phys.* **2005**, *98*, 094312.
[46] M. C. Biesinger, *Appl. Surf. Sci.* **2022**, *597*, 153681.
[47] M. Grodzicki, *Materials Proceedings* **2020**, *2*, 30.
[48] M. Grodzicki, P. Mazur, S. Zuber, J. Brona, A. Ciszewski, *Appl. Surf. Sci.* **2014**, *304*, 20.
[49] K.-K. Lee, Z. Cai, K. Ziemer, W. A. Doolittle, *J. Cryst. Growth* **2009**, *311*, 4001.
[50] H.-S. Kang, M. Siva Pratap Reddy, D.-S. Kim, K.-W. Kim, J.-B. Ha, Y. S. Lee, H.-C. Choi, J.-H. Lee, *J. Phys. D: Appl. Phys.* **2013**, *46*, 155101.
[51] R. Sohal, P. Dudek, O. Hilt, *Appl. Surf. Sci.* **2010**, *256*, 2210.
[52] Y. Zhong, Y. Zhou, H. Gao, S. Dai, J. He, M. Feng, Q. Sun, J. Zhang, Y. Zhao, A. DingSun, H. Yang, *Appl. Surf. Sci.* **2017**, *420*, 817.
[53] F. Le Roux, N. Possémé, P. Burtin, S. Barnola, A. Torres, *Microelectron. Eng.* **2020**, *228*, 111328.
[54] V. Thakur, S. M. Shivaprasad, *Appl. Surf. Sci.* **2015**, *327*, 389.
[55] D. A. Zatsepin, D. W. Boukhvalov, A. F. Zatsepin, *Appl. Surf. Sci.* **2021**, *563*, 150308.
[56] F. González-Posada, J. A. Bardwell, S. Moisa, S. Haffouz, H. Tang, A. F. Braña, E. Muñoz, *Appl. Surf. Sci.* **2007**, *253*, 6185.
[57] C. V. Ramana, D. Das, G. Gutierrez, F. S. Manciu, V. Shutthanandan, *J. Mater. Sci.* **2022**, *57*, 11170.
[58] Q. Shi, S. Wei, F. Shi, T. Chen, M. Zhao, M.-k. Lee, *J. Mater. Res. Technol.* **2024**, *30*, 2099.
[59] S. S. Kushvaha, M. S. Kumar, M. Maheshwari, A. K. Shukla, P. Pal, K. K. Maurya, *Mater. Res. Express* **2014**, *1*, 035903.
[60] C. V. Ramana, A. Ait-Salah, S. Utsunomiya, J. F. Morhange, A. Mauger, F. Gendron, C. M. Julien, *J. Phys. Chem. C* **2007**, *111*, 1049.
[61] C. V. Ramana, A. Ait-Salah, S. Utsunomiya, A. Mauger, F. Gendron, C. M. Julien, *Chem. Mater.* **2007**, *19*, 5319.
[62] N. Fairley, A. Carrick, *The Casa Cookbook*, Acolyte science, Cheshire **2005**.